VALIDATION AND VERIFICATION OF DECOMPOSITION MODEL BASED ON EMBEDDED FREE SURFACE METHOD FOR OBLIQUE WAVE SEAKEEPING SIMULATIONS

Vuko Vukčević (Faculty of Mechanical Engineering and Naval Architecture, Croatia)
Hrvoje Jasak (Faculty of Mechanical Engineering and Naval Architecture, Croatia)

1 SUMMARY

In this paper validation and verification of a KCS model in oblique seas is presented for five headings. Validation is performed by comparing added resistance, heave, roll and pitch motions with experimental data. For each test case, grid refinement study is carried out and the corresponding grid uncertainty is calculated. Periodic uncertainty using moving window FFT is calculated. The decomposition model is based on SWENSE (Spectral Wave Explicit Navier–Stokes Equations) method and implicit relaxation zones, with embedded free surface approach via implicit interface–corrected interpolation schemes. The method provides one–cell–sharp jump of dynamic pressure and density across the free surface for arbitrary polyhedral grids. Implicitly redistanced Level Set equation is used for interface capturing, while the $k-\omega$ SST model is used for turbulence. The method is implemented in the `Naval Hydro pack`, based on foam–extend, a fork of the open source software OpenFOAM.

2 INTRODUCTION

With a decrease in CPU cost–performance ratio and recent regulations regarding energy efficient marine transport, the focus in marine CFD is shifting to more complex flows including seakeeping and manoeuvring [7, 12] of ships. Heave and pitch motions of a ship in head waves are well investigated using CFD [10, 2], although the emphasis nowadays is on the added resistance of a ship in waves. Detailed validation and verification of CFD simulations of ships in oblique waves with variable heading are still to be investigated.

This paper presents validation and verification for seakeeping CFD simulations of a KCS in oblique waves, where each of the five test cases has been carried out, results compared to experimental data and verified with grid refinement studies. Grid and periodic uncertainties are also calculated, and the emphasis is generally given to added resistance due to its practical importance.

The paper is organised as follows. The decomposition CFD model is briefly outlined, followed by a brief description of uncertainty assessment. A global overview of the results is given and the paper is finalized with a short conclusion.

3 APPROACH

The computational method used in this work is based on the recently developed decomposition model for naval hydrodynamics [14]. Solution decomposition via SWENSE approach [3] ensures facilitated incident wave transport, while the domain decomposition via implicit relaxation zones [6] prevents wave reflection. Implicitly redistanced Level Set method is used for interface capturing [13], and the embedded free surface approach is used to ensure infinitesimally sharp interface for density and dynamic pressure.

In SWENSE, primitive variables are decomposed into incident (potential) flow solution and perturbation (diffracted) solution [3]:

$$\xi = \xi_I + \xi_D \,, \tag{1}$$

where ξ represents an unknown field, with index I denoting its potential flow incident part and index D denoting the diffracted (perturbation) part. Such decomposition allows one to solve for a fully non–linear CFD solution for the perturbation solution, treating the incident flow field explicitly. Using ordinary second–order accurate convection and time–derivative schemes for incident fields, incident wave is easily propagated without excessive numerical damping and need for finely resolved grid in the far–field. Thus, the SWENSE approach facilitates introduction of regular waves in the CFD calculation.

In order to prevent wave reflection from the far–field boundaries, implicit relaxation zones [6] are introduced. The relaxation zones are positioned near the far–field boundaries, where they damp out the perturbation solution, thus leaving only potential flow solution and preventing wave reflection. This damping is achieved on a matrix level via additional sink terms with smooth blending using a spatially–defined exponential blending function.

Implicitly redistanced Level Set method [13], highly suitable for SWENSE decomposition, is used for interface capturing. Additional diffusion and source/sink terms in the transport equation force the Level Set field to remain a signed distance function during its transport. Hence, no additional redistancing via direct calculation or introduction of the Eikonal redistancing equation is necessary.

Embedded free surface approach [15] allows one to formulate a single two–phase incompressible system of equations coupled at the water/air interface via density and pressure jump conditions. Following Huang et al. [4], jump conditions are used to derive interface–corrected interpolation schemes for cells in the vicinity of the free surface, ensuring one–cell–sharp jump in density and dynamic pressure:

- Dynamic pressure jump condition:

$$p_d^- - p_d^+ = -(\rho^- - \rho^+)\mathbf{g}_\bullet\mathbf{x}\,, \tag{2}$$

  where $p_d = p - \rho\mathbf{g}_\bullet\mathbf{x}$ is the dynamic pressure, and superscripts + and − denote field values infinitesimally close to the free surface from water and air sides, respectively. Similarly, ρ^- is the constant air density and ρ^+ is the constant water density. $\mathbf{g}$ is the gravitational acceleration and $\mathbf{x}$ is the free surface position vector.

- Dynamic pressure gradient jump condition:

$$\frac{1}{\rho^-}p_d^- - \frac{1}{\rho^+}p_d^+ = 0\,. \tag{3}$$

Reader is referred to Vukčević and Jasak [15] for a detailed derivation of jump conditions, two–phase governing equations and interface–corrected numerical schemes.

Turbulence is modelled with two–equation $k-\omega$ SST eddy–viscosity model [8].
Second–order accurate polyhedral Finite Volume (FV) method [5] is used to discretise governing equations. As the polyhedral FV method uses a compact computational stencil, interface–corrected schemes arising from dynamic pressure jump conditions (2) and (3) are used only for cells in the immediate vicinity of the free surface, while ordinary discretisation is employed for fully submerged or fully dry cells. Time derivative terms for perturbation fields are discretised with first–order accurate implicit Euler scheme (due to stability issues on some grids), while time derivative terms for explicit, incident fields are discretised with a blend of Crank–Nicholson and Euler schemes. This combination proved to be accurate in previous studies. Convective terms for incident and diffracted fields are discretised with linear and linear upwind interpolation, respectively. All diffusion terms are discretised using linear interpolation with limited non–orthogonal correction in over–relaxed form [5]. Theoretically, second–order spatial accuracy and a blend of first– and second–order temporal accuracy is achieved.

Six–degrees–of–freedom (6 DOF) rigid body motion equations [1] are introduced to model ship motion, where the rotation is formulated in quaternion form to prevent the gimbal lock phenomenon. After the solution of 6 DOF equations, the whole computational grid is moved and grid motion fluxes are calculated, where far–field relaxation zones naturally account for moving grids.

6 DOF and grid motion are tightly coupled to the fluid flow solution via forces and moments acting on the body, prescribed velocity of the body and grid motion fluxes. In order to resolve this coupling, fluid flow and 6 DOF equations are solved using Picard iterations. First, interface capturing Level Set equation is solved, followed by a momentum equation. The pressure–velocity coupling for the current interface location is resolved in the inner PISO loop with 3 or 4 correctors. After obtaining a converged flow field including turbulence, 6 DOF equations are solved and the grid is moved accordingly. With updated grid motion fluxes and velocity boundary conditions for the body, a new estimate of the flow field is calculated. The procedure is repeated at least 5 times to damp out oscillatory convergence of rigid body accelerations.

4 VALIDATION

Validation of the model is performed by simulating five wave encounter angle cases: head waves (C1), bow waves (C2), beam waves (C3), quartering waves (C4) and following waves (C5) requested by the Workshop [9] for the KCS model at design Froude number, and comparing the added resistance, heave, roll and pitch motions with experimen-

tal data. Reader is referred to Workshop's website [9] for detailed case settings and post processing instructions. Three unstructured grids with approximately 1 200 000, 1 900 000 and 3 200 000 cells are used. Each grid extends approximately $1L_{PP}$ in front of the ship, $2.5L_{PP}$ behind the ship and $1.5L_{PP}$ from the portside and starboard. Results presented in this section are obtained by performing moving window FFT on temporal signals for the finest grid, while the verification study with grid and periodic uncertainty estimates is presented afterwards.

4.1 Added resistance

Mean value, first and second order harmonics of the total resistance coefficient are presented in Fig. 1 for all wave encounter angles χ ($\chi = 0°$ representing head waves and $\chi = 180°$ representing following waves). Mean value of the total resistance deviates 2% and 4% from experimental results for head and bow waves respectively, while CFD significantly over–estimates added resistance in beam, quartering and following waves. Note that the measured experimental value for the mean resistance is smaller for beam waves compared to calm water condition, which is considered peculiar. First order of the total resistance is significantly higher in CFD compared to experimental results, except for the beam waves case. Comparing the head wave case from seakeeping in oblique waves (KCS 2.11 case set), with the experimental results of seakeeping in head waves (KCS 2.10 case set, [9]), measured first order of added resistance is significantly under–predicted.

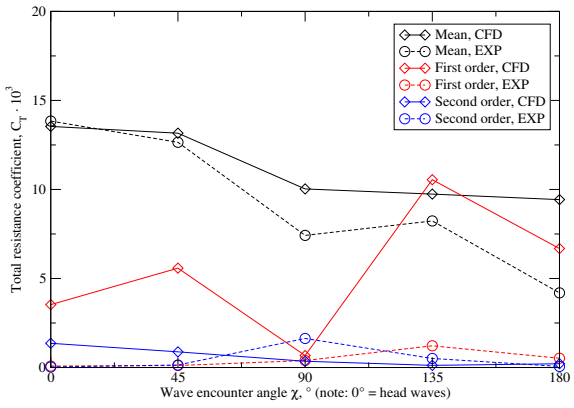

Figure 1: Total resistance coefficient harmonics, C_T for all wave encounter angles.

4.2 Heave motion

Mean value, first and second order harmonics of the dimensionless heave are presented in Fig. 2 for all wave encounter angles. The mean value of heave is well predicted for head, bow and following waves, with larger discrepancies for beam and quartering waves. First order heave compares well with experimental results for all wave wave encounter angles, with average relative error of 13%, excluding the following wave case with large relative error due to small measured motion. CFD slightly over–predicts heave motions, except for the following waves case. Small second order effects are also well predicted.

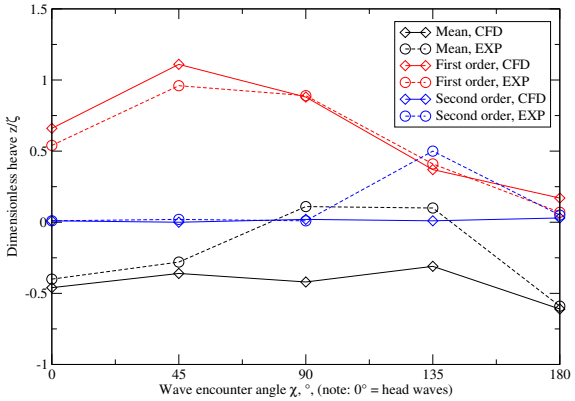

Figure 2: Dimensionless heave harmonics, z/ζ for all wave encounter angles.

4.3 Roll motion

Mean value, first and second order harmonics of the dimensionless roll are presented in Fig. 3 for all wave encounter angles. The mean value of roll in CFD does not compare well to the experimental results, where significant mean values are obtained for head and following wave cases. First order of the roll motion is under–predicted for bow and following seas, while the CFD simulation of beam waves over–predicts roll motion.

4.4 Pitch motion

Mean value, first and second order harmonics of the dimensionless pitch are presented in Fig. 4 for all wave encounter angles. Compared with the experimental results, mean value of pitch motion has opposite sign in CFD. It is possible this is a post processing error, since experimental results report "bow up" condition for the calm water (C0) test case, whereas

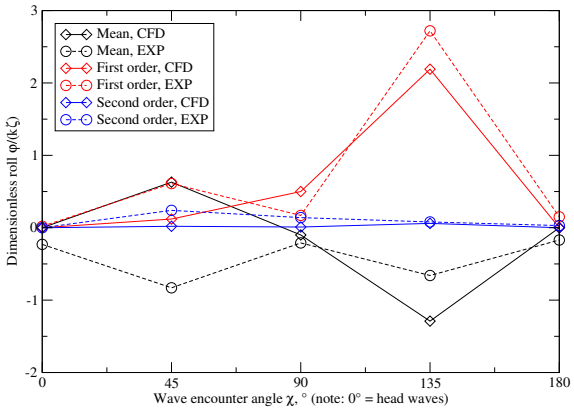

Figure 3: Dimensionless roll harmonics, $\phi/(k\zeta)$ for all wave encounter angles.

other experimental tests with similar model report "bow down" at design Froude number. The average relative error for the first order pitch motion is approximately 16%, with the exception of beam waves case where small pitch motions are measured both in CFD and experiments. Considering their small amplitude, second order effects are in good agreement with experimental results.

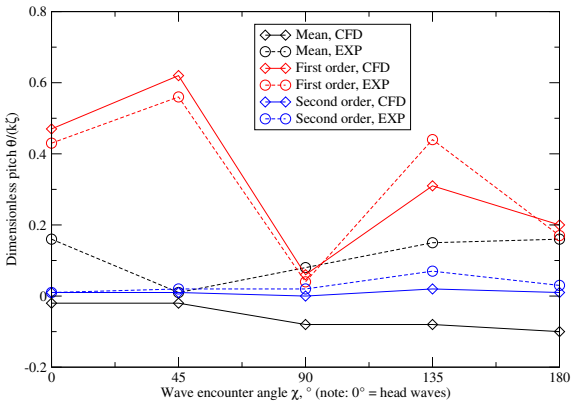

Figure 4: Dimensionless pitch harmonics, $\theta/(k\zeta)$ for all wave conditions.

5 VERIFICATION

We shall first examine periodic uncertainty and then calculate grid uncertainty, for each test case.

5.1 Periodic uncertainty assessment

As the seakeeping CFD simulations are almost exclusively carried out in the time domain, appropriate number of periods needs to be calculated. In highly non–linear flow problems such as seakeeping of a ship in oblique waves, minimum number of required periods needs to be assessed. For this reason, we perform a moving window FFT on each signal, which provides useful information about convergence of particular harmonics. The convergence for all variables (harmonic amplitudes and phases for resistance, heave, roll and pitch, for all cases) is found to be oscillatory. Hence, we calculate periodic uncertainty in the same way as the oscillatory grid uncertainty [11]:

$$U_P = 0.5|S_U - S_L|\,, \tag{4}$$

where S_U is the maximum value, and S_L is the minimum value of the moving window FFT plot over the final region used for post processing, usually last 5 to 10 encounter periods. For most of the phases in oblique wave cases, a small drift (e.g. approximately 0.15 degrees for first order added resistance in bow waves case) is revealed using moving window FFT, hence the uncertainty calculation is not possible.

Periodic uncertainties for the mean and first order harmonics of resistance, heave, roll and pitch are smaller than 1% of the finest grid result for most cases. Periodic uncertainties for higher order (third and fourth) harmonics for added resistance are below 7%. Some higher order motion amplitudes have periodic uncertainties of up to 65%, e.g. fourth order roll motion in bow waves. However, this is expected as the measured CFD value of 4th order roll is 3 orders of magnitude smaller than corresponding first order. Periodic uncertainties for higher order harmonics could be lowered by simulating more encounter periods.

5.2 Grid uncertainty assessment

Grid convergence and uncertainty is assessed following [10], using results from 3 (non–systematically) refined grids. A mixture of monotonically–, oscillatory– and non–converging solutions is obtained as in previous studies concerning seakeeping of the KCS ship [10], hence the grid uncertainty is estimated as a difference in maximum and minimum solutions:

$$U_G = |S_U - S_L|\,, \tag{5}$$

5.2.1 Added resistance grid uncertainties

The average grid uncertainty U_G for the mean value of resistance is approximately 10% of the finest grid result. Grid uncertainty for the first order harmonic of the resistance is less than 3%, except for the beam waves C3 case where $U_G = 59\%$.

5.2.2 Heave grid uncertainties

For the mean value of heave, grid uncertainty ranges from 2% for head waves C1 case to 27% for quartering waves C4 case. Grid uncertainties for first order harmonics of heave are smaller than 2%, except for the following waves case where the grid uncertainty is 18%.

5.2.3 Roll grid uncertainties

Mean value of roll has grid uncertainties of 7% for bow waves and 3% for quartering waves. Beam waves case has high grid uncertainty of 63%, which should be further explored. Average grid uncertainty for first order roll motion for bow, beam and quartering waves is approximately 4%, with higher uncertainties in head and following waves due to negligible roll response.

5.2.4 Pitch grid uncertainties

Grid uncertainties for first order pitch motion are below 2%, except for the beam waves case with small pitch response. Grid uncertainties for mean values are 6% and 2% for quartering and following waves, respectively, with higher values for other cases (up to 63% for bow waves), caused by small mean pitch motion.

6 HARDWARE AND SIMULATION TIMES

Simulations were performed on a cluster with 7 nodes: CPU - 2x Intel Xeon E5-2637 v3 4-core, 3.5 GHz, 15MB L3 Cache, DDR4-2133.
As an example, the finest grid (3.2 million cells) simulation of the bow waves case has been performed using 56 cores. 7 motion correctors were used with fixed time step of 0.004 s corresponding to approximately 225 time steps per encounter period. Maximum CFL number was ranging from 55 to 70 during the simulation. Simulation lasted 40.2 hours for 60 encounter periods, equalling 40 minutes of clock time per encounter period.
The most computationally expensive simulation has been the following wave test case because the encounter period is highest. With same time–step and number of cores as in the bow waves case, it took 4.5 hours per encounter period, approximately 104 hours for 22 encounter periods. It should be noted that for this test case, a significant amount of CPU time has been spent on output operations for visualisation purposes.

7 CONCLUSION

This paper describes a detailed validation and verification of the decomposition model with embedded free surface approach for seakeeping simulations in oblique waves. The computational model is implemented in the `Naval Hydro pack` based on foam–extend C++ library, a community driven fork of OpenFOAM software.
Five test cases of the KCS ship model heaving, rolling and pitching in oblique seas are simulated: head, bow, beam, quartering and following waves. Validation is performed by comparing mean to fourth order harmonics of added resistance, heave, roll and pitch motions to the experimental data, while the verification is performed via grid refinement studies and periodic uncertainty assessment using moving window FFT.
Compared with experimental results, the mean value of the added resistance is well predicted for the head and bow waves, while beam, quartering and following waves indicate larger discrepancies. First order amplitudes of the added resistance are significantly over–predicted by the CFD. CFD simulations were performed with surge fixed condition as recommended by the Workshop organisers, while the experiments were performed using surge free mount system consisting of a spring and a damper, which we believe is the main reason for discrepancies. Periodic uncertainties for the added resistance coefficient are smaller than 1% for all mean, first and second orders, while for the third and fourth orders the largest periodic uncertainty is approximately 7% of the fine grid solution. Grid uncertainties for the mean value of the added resistance are between 6% and 13%. First order added resistance coefficients have periodic uncertainties below 3%, except for the beam waves case with high periodic uncertainty of 58%.
Heave, roll and pitch motions are generally in better agreement with experimental results compared to the added resistance coefficient. The most notable discrepancies within motions between present CFD results and experimental results are:

1. Mean value of heave motion for beam and bow waves have different signs,

2. Mean value of roll motion in bow waves has different sign,

3. First order roll motion is under–predicted in CFD for bow waves and over–predicted for beam waves,

4. Mean value of pitch motion has different signs for all wave conditions.

As reported, periodic and grid uncertainties for the motions are low, considering the complexity of the cases and usage of non–systematically refined unstructured grids.
Authors hope to investigate the above mentioned discrepancies for motions and added resistance at the Workshop.

References

[1] P. M. Carrica, R. V. Wilson, R. W. Noack, and F. Stern. Ship motions using single–phase level set with dynamic overset grids. *Comput. Fluids*, 36:1415–1433, 2007.

[2] T. Castiglione, F. Stern, S. Bova, and M. Kandasamy. Numerical investigation of the seakeeping behavior of a catamaran advancing in regular head waves. *Ocean Eng.*, 38:1806–1822, 2011.

[3] P. Ferrant, L. Gentaz, and D. Le Touzé. A new RANSE/Potential Approach for Water Wave Diffraction. In *Proc. Numerical Towing Tank Symposium, NuTTS*, September 2002.

[4] J. Huang, P. M. Carrica, and F. Stern. Coupled ghost fluid/two–phase level set method for curvilinear body–fitted grids. *Int. J. Numer. Meth. Fluids*, 44:867–897, 2007.

[5] H. Jasak. *Error Analysis and Estimation for the Finite Volume Method with Applications to Fluid Flows*. PhD thesis, Imperial College of Science, Technology & Medicine, London, 1996.

[6] H. Jasak, V. Vukčević, and I. Gatin. Numerical Simulation of Wave Loads on Static Offshore Structures. In *CFD for Wind and Tidal Offshore Turbines*, pages 95–105. Springer Tracts in Mechanical Engineering, 2015.

[7] L. Larsson, F. Stern, and M. Vissoneau. *Numerical Ship Hydrodynamics: An assessment of the Gothenburg 2010 workshop*. Springer, 2013.

[8] F. R. Menter. Two-equation eddy-viscosity turbulence models for engineering applications. *AIAA J.*, 32(8):1598–1605, 1994.

[9] National Maritime Reasearch Inistitute (NMRI). Tokyo 2015: A Workshop on CFD in Ship Hydrodynamics. `http://www.t2015.nmri.go.jp/`, 2015. [Online; accessed 20 August 2015].

[10] C. D. Simonsen, J. F. Otzen, S. Joncquey, and F. Stern. EFD and CFD for KCS heaving and pitching in regular head waves. *J. Mar. Sci. Technol.*, 18:435–459, 2013.

[11] F. Stern, R. V. Wilson, H. W. Coleman, and E. G. Paterson. Comprehensive Approach to Verification and Validation of CFD Simulations–Part 1: Methodology and Procedures. *J. Fluids. Eng*, 123(4):793–802, 2001.

[12] F. Stern, J. Yang, Z. Wang, H. Sadat-Hosseini, M. Mousaviraad, Bhushan S., and T. Xing. Computational Ship Hydrodynamics: Nowadays and Way Forward. In *Proceedings of the 29th Symposium on Naval Hydrodynamics*, pages 1–73, August 2012.

[13] Y. Sun and C. Beckermann. Sharp interface tracking using the phase–field equation. *J. Comput. Phys.*, 220:626–653, 2007.

[14] V. Vukčević and H. Jasak. Decomposition Model for Naval Hydrodynamic Applications, Part I: Computational Method. *Submitted to Ocean Engineering*, ??:???–???, 2015.

[15] V. Vukčević and H. Jasak. Embedded Free Surface Method in Polyhedral Finite Volume Framework: Part I: Computational Method. *Submitted to Journal of Computational Physics*, ??:???–???, 2015.